GREEN WATER LOADING ON A DECK STRUCTURE

M.Greco,
Dep.of Marine Hydrodynamics, NTNU
7491, Trondheim, Norway
Email: marilena@marin.ntnu.no

O.M.Faltinsen
Dep.of Marine Hydrodynamics, NTNU
7491, Trondheim, Norway
Email: oddfal@marin.ntnu.no

M.Landrini
INSEAN, The Italian Ship Model Basin
Via di Vallerano 139, 00128, Roma, Italy
Email: maulan@waves.insean.it

At the previous Workshop, a numerical investigation of water-on-deck phenomena was presented by the same authors. A two-dimensional problem was considered. The effect of main wave- and body-parameters was studied. The fully nonlinear problem was solved by boundary-integral equations. Here, we discuss a continuation of that activity. Results from an on-going experimental investigation are presented, together with the analysis of the interaction of the fluid on the deck with superstructures.

Experiments Two-dimensional water-on-deck (w.o.d.) model tests are on-going in a narrow wave flume (13·5 m long, 1 m deep, 0·6 m wide). Incoming waves are generated by a flap wavemaker hinged at 0·1 m from the bottom. The selected body-parameters are: draft $D = 0{\cdot}2$ m, length $L = 1{\cdot}5$ m, freeboard $f = 0{\cdot}05$ m. The bottom corner at the bow was rounded with a radius of curvature 0·08 m to avoid significant vortex shedding. Body motions are restrained. Since the generated wave system is highly transient, with the first crest generally steeper than the following ones, we decided to focus on the first w.o.d. event.

Fig. 1 is representative of the behavior when the fluid invades the deck. The nominal incoming wave length is $\lambda = 2$ m and the wave height $H = 0{\cdot}16$ m. At the beginning the fore-part of deck remains dry, and the shipping of water starts in the form of a rounded jet plunging directly onto the deck. A cavity is formed with air trapped inside. This behavior has been observed in all the test-conditions we studied. Moreover, though for the case shown the jet hits the deck rather close to the bow edge, cases are recorded were the fluid organizes itself to plunge on the deck further from the bow. Finally, in a few cases even blunter impacts have been observed. In all cases, the front view of the event confirmed the two-dimensionality of the phenomenon and excluded that the cavity formation is related to localized three-dimensional instabilities. As a consequence, the initiation of deck-wetting should be characterized by localized high impact pressures. In the reported example, the time scale involved is rather short, about 0·12 s, and at the instant of impact the entrapped cavity has length $l_{\rm cav}/D \simeq 0{\cdot}16$ and height $h_{\rm cav}/D \simeq 0{\cdot}05$. This fluid behavior was not mentioned in the two–dimensional experiments reported in Cozijn (1995). This may be due to the small time and space scales involved. A consequence of the presence of the cavity is that capacity wave probes do not estimate correctly free-surface height.

As time increases (*cf.* bottom plots in Fig. 1) two horizontal jets develop after the impact of the plunging fluid front. One of the two moves backwards towards the bow edge and reduces the cavity volume. The other propagates forward along the deck and increases the wetting velocity relative to a dam-breaking type analysis. As time passes, the cavity moves forward, convected together with the shipped water. Also, the water level above the cavity increases and contributes to squeeze it. This combined actions are responsible, together with surface tension, of the fragmentation of the cavity, though we cannot document this evolution because of the limited frame rate of the video camera.

We used fluorescent material injected in front of the bow edge to detect a possible vortex-shedding in the initial stage of the phenomenon. In particular, we observed that, after the air entrapment, when the cavity starts to move forward, the gravity has already organized the run–down of the fluid in front of the model, preventing the beginning of vortex shedding, at least of strength large enough to be detected by the used method. At this stage, the flow pattern can be sketched as one stream wetting the deck and one involved in the run–down, with negligible cross-flow at the bow edge.

These new features observed in the experiments are not modeled in our computations, where the fluid is allowed to wet the deck as soon as it exceeds the freeboard. A better modeling would probably require the use of a Kutta-like condition, with the fluid leaving tangentially the front bow-edge, and the description of the jet plunging onto the deck. The free surface shape close to the separation point at the bow can be found by a local analysis, Zhao & Faltinsen (1998). This gives $z_1 = C(t)x_1^{2/3}$. Difficulties related to high fluid velocity are expected during impact, and may be alleviated by locally using a Wagner-type of analysis. The final collapse of the cavity would require other methods.

In spite of this, we applied our method to simulate the experiments, and results (solid lines) for later stages of the phenomenon are compared in Fig. 2 with experimental free-surface profiles, ∘. In particular, to reproduce as close as possible the experimental set-up, the actual wave flume has been modeled numerically and the motion of the physical flap has been used to drive the numerical one. However a mathematical damping region different from the physical wave beach was used. This difference matters initially when a seiching

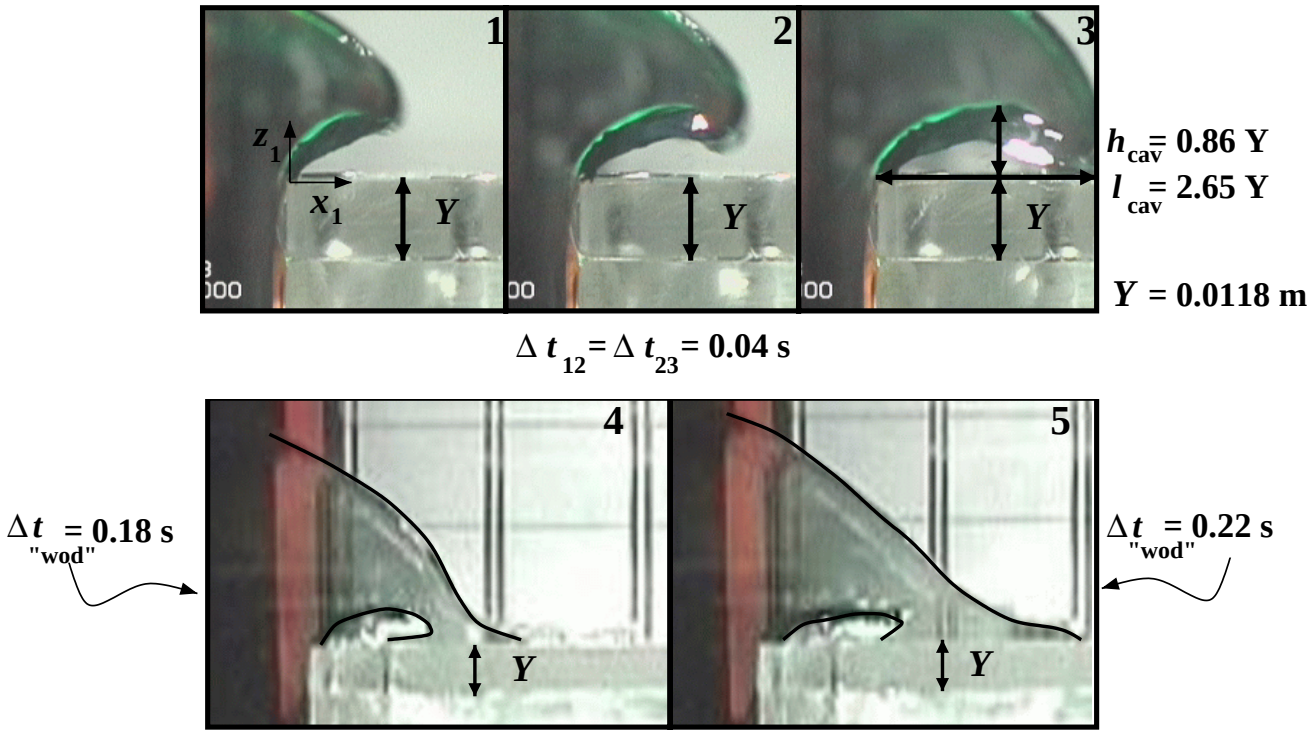

Figure 1. Water-on-deck at the bow of a 2-D ship. Top: initial stage of the wetting. Bottom: cavity formation and transition to dam-breaking type of flow.

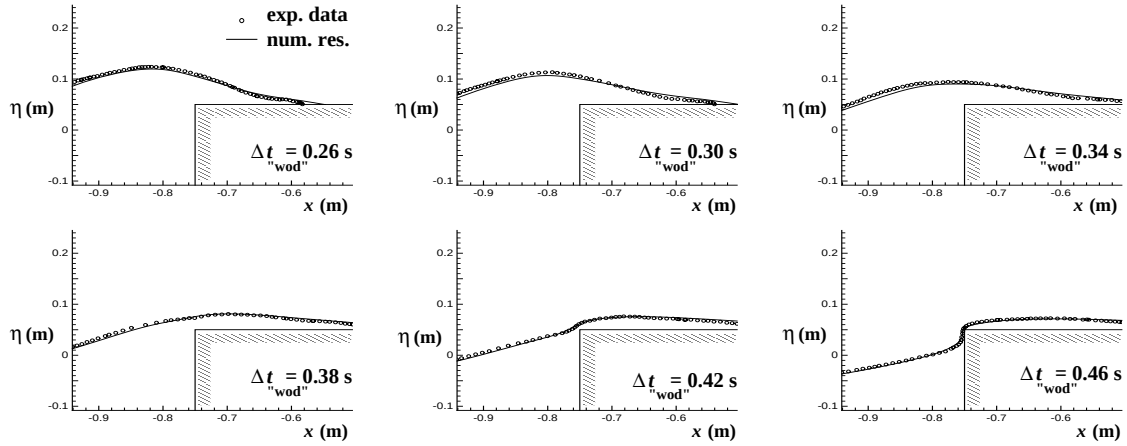

Figure 2. Water-on-deck on a 2-D ship. Comparison of numerical simulation with experimental free-surface profiles. Nominal incoming waves conditions: $\lambda = 2$ m, $H = 0{\cdot}16$ m.

motion is set up in the tank. However the seiching amplitude is small and minimized by the automatically controlled wavemaker. Apparently, though we neglected the details of the initial stages of water shipping and of the wave beach, results agree well with measured profiles (obtained through the digital record of the video camera) with the exception of the wave front region were the numerical method predicts a higher velocity. This suggests that the gross flow evolution is not significantly affected by the phenomena connected with the initial plunging. The instant t_{wod} in Figs. 1–2 indicates the instant of water-on-deck starting in the numerical simulation. Future tests will include the impact of the green water on a vertical deck structure. Relevant numerical studies of the phenomenon are reported in the following text.

Fluid–structure interaction Greco *et al.* (2000) studied the two-dimensional impact of water on a rigid vertical superstructure after a dam break. Here, we investigate the influence of hydroelasticity. The left plot in Fig. 3 gives an example of longitudinal steel stiffeners adopted for the deck house of a FPSO unit. We focus on the effects of those between deck 8 and deck 9 by using an equivalent Euler beam. The upper portion of the deck house is assumed rigid. The cross section is shown in the right plot. Recent accidents for FPSO units documented in Ersdal & Kvitrud (2000), suggest

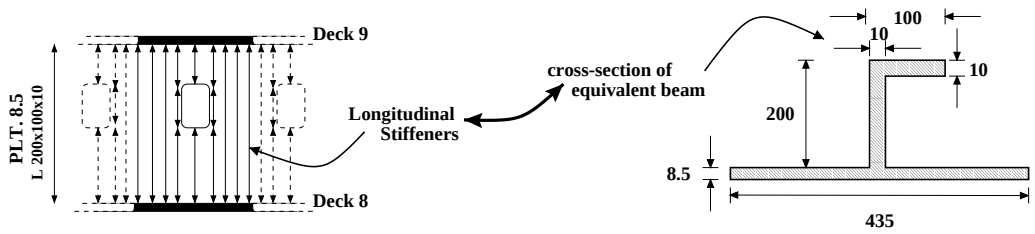

Figure 3. Example of stiffeners of a deck structures. Lengths are in millimeters.

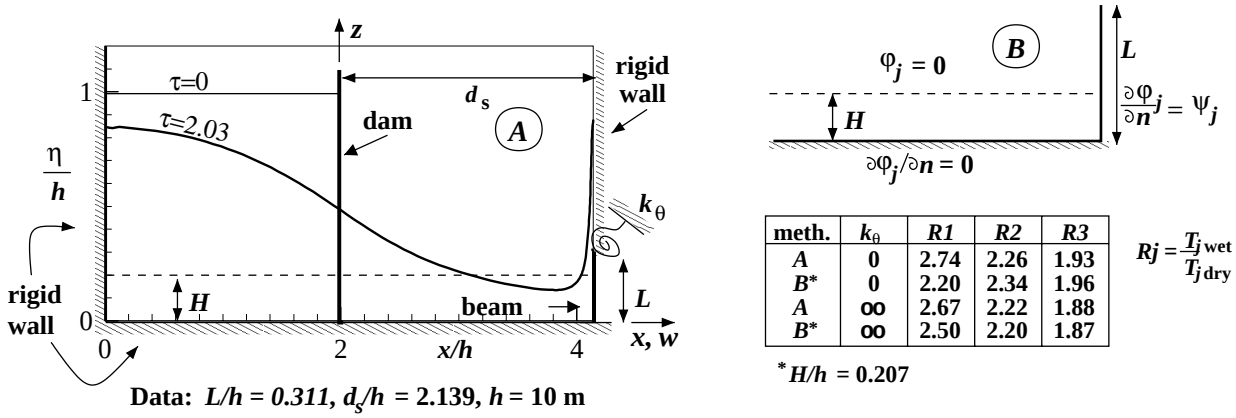

meth.	k_θ	R1	R2	R3
A	0	2.74	2.26	1.93
B*	0	2.20	2.34	1.96
A	∞	2.67	2.22	1.88
B*	∞	2.50	2.20	1.87

$Rj = \frac{T_j\,\text{wet}}{T_j\,\text{dry}}$

* $H/h = 0.207$

Figure 4. Impact with a vertical wall after a dam-break (left). In the table, the 'exact' solutions (A) for natural periods are compared with results from the simplified analysis (B) sketched in the top-right plot.

to use a freeboard exceedence of 10 m. The flow is originated as the breaking of a dam located at the bow, with height $h = 10$ m and length $2h$ (*cf.* Fig. 4). The beam is located $d_s = 2{\cdot}139h$ from the dam, with length $L = 0{\cdot}311h$. The lower edge is clamped, while rotations at the upper edge are constrained by a spring with constant k_θ. The deformation $w(z,t)$ of the beam is expressed in terms of the known dry modes $\psi_j(z)$ of the beam with unknown amplitudes $\zeta_j(t)$. Structural damping is neglected.

The fluid-structure interaction is studied by coupling the nonlinear potential fluid model with the linear beam. For a given time, w and w_t are known and the b.v.p. for the potential φ is solved by imposing $\varphi_n = w_t$ along the beam. For the hydrodynamic pressure at the wall, φ_t is found by solving a similar b.v.p. with the exception of the boundary condition at the beam, where the Neumann condition is substituted by a non-homogeneous Robin condition. The latter follows by inserting the condition for φ_{tn} into the beam equation and represents the fluid-structure coupling. Once the φ_t is known, w_{tt} can be evaluated and fluid motion and structural deformation can be prolonged in time. A similar procedure was applied by Tanizawa (1999) to analyze the impact of a flexible body on a free surface.

The initial conditions, $\tau = t\sqrt{g/h} = 0$, are shown in Fig. 4, together with a later free-surface configuration, when the wetted portion of the vertical wall is almost $3L$. The flow generated after the impact is characterized by a narrow jet of water rising along the wall, also observed in case of rigid wall.

The numerical solution can be negatively affected by a variety of difficulties: spatial and time resolutions decrease progressively for higher-order modes and confluence of different boundary conditions at the edges of the beam implies locally a poorer convergence. Therefore, a simplified analytical analysis (top-right plot in Fig. 4) is also considered to check the present results. The incoming water is approximated by a strip of fluid with constant height H, and the potential φ_j due to j-th mode oscillations with unit amplitude is computed with $\varphi_j = 0$ along the free surface. A solution is found by separation of variables and a Fourier expansion of the mode over the wetted surface. The height H is a free parameter chosen by the following considerations. In the approximate problem, it is found that the fluid further away than $\sim 0{\cdot}79L$ from the beam is practically not affected by vibrations. Therefore H is determined by imposing that masses of fluid involved in the approximate and exact problems are the same. In this procedure, particles above the beam are neglected because their role in the hydroelastic problem is expected to be small. This procedure gives an $H/h = 0{\cdot}207$. The ratio natural wetted-period to natural dry-period $Rj = T_{j\text{wet}}/T_{j\text{dry}}$ is computed and compared with results obtained by the 'exact' problem. This comparison is tabulated for $j = 1,2,3$ in Fig. 4 for $k_\theta = 0, \infty$ and shows a promising agreement, more evident for the higher modes, as we can expect since their sensitivity to the fluid details is smaller. Left plots in Fig. 5 give the time evolution of ζ_j for the first two modes, in the case of $k_\theta = 0$. Late stages are presented for $j = 1,\ldots,4$. After the beam is completely wetted, $\Delta\tau_{\text{imp}} \simeq 0{\cdot}12$, the modes oscillate with almost constant period and amplitude. Both the value of ζ_j and the amplitude of oscillations decrease as the order of mode increases. This behavior does not change substantially when the parameter $K_\theta = k_\theta L/EI$ is varied (EI is the beam

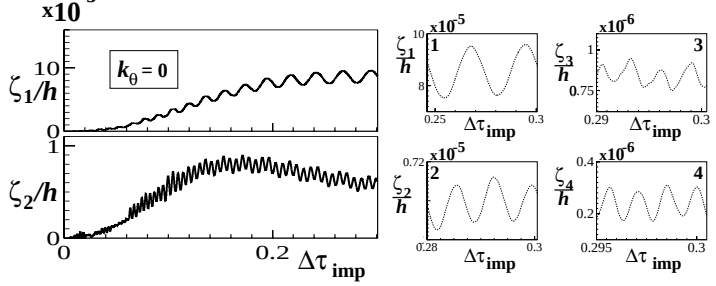

K_θ	0	6	24	oo
R1	2.74	2.73	2.67	2.67
R2	2.26	2.25	2.23	2.22
R3	1.93	1.93	1.88	1.88
R4	1.71	1.70	1.67	1.67

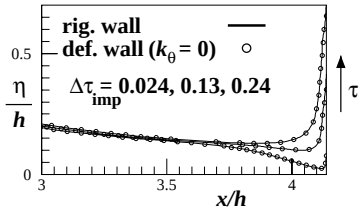

Figure 5. Left: Amplitude of the first four modes as a function of time. Table: ratio of natural wetted-periods to natural dry-periods for the first four modes of the beam. $K_\theta = k_\theta L/EI$. Right: free surface for three different instants after the impact (solid lines: rigid wall, ∘: $k_\theta = 0$).

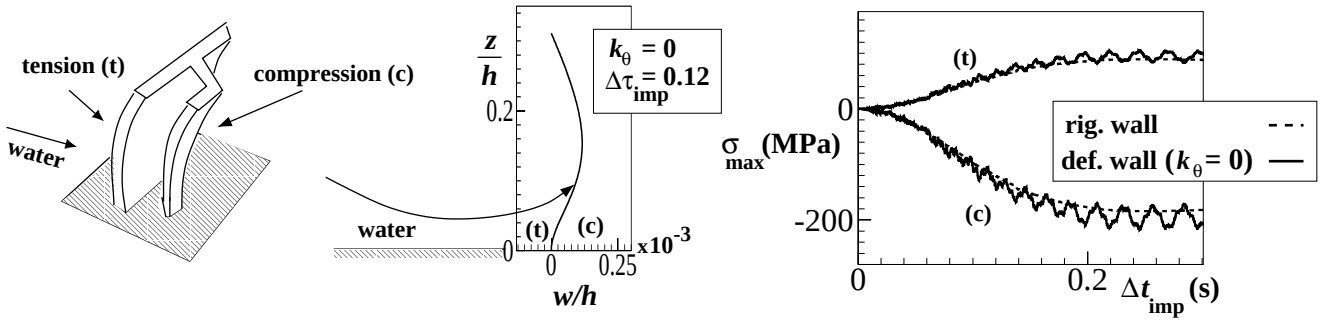

Figure 6. Left: sketch of the loaded beam. Center: deformation of the beam for $\Delta\tau = 0{\cdot}12$ after the impact. Right: maximum tension and compression stresses as a function of time. Quasi-steady (dashed lines) and hydroelastic (solid lines) analyses ($k_\theta = 0$).

bending stiffness). Qualitatively we observe smaller amplitudes as it increases and a minor influence for higher modes, which are less sensitive to the boundary conditions. In general, Rj decreases as K_θ increases and it is smaller for higher j (see the table). The highest natural wetted-period changes from $\sim 0{\cdot}018$ to $\sim 0{\cdot}026\sqrt{h/g}$ as we go from $K_\theta = \infty$ to 0. This means $T_{1\text{wet}}$ is small compared to the time duration for the beam to be wetted. It implies that the hydroelasticity does not play an important role for the resulting maximum strains (*cf.* Faltinsen (2001)).

The rigid wall results, solid lines, are compared with the clamped-supported beam results, ∘, in the right plot of Fig. 5 for the free-surface configurations at three instants of time after the impact. The overall pattern is not affected by wall deformation.

In Fig. 6, we analyze maximum stresses on the beam based on hydroelastic and quasi-steady analyses. The latter means rigid structure from a hydrodynamic point of view and resulting static structural deformations. Fifteen modes are used in the calculations. For the considered cases, maxima are always observed at the bottom end. In particular, left plot, the fluid-induced bending moment gives tension stresses (t) in the wetted side, and compression stresses (c) in the opposite side. The deformation of the beam for $\Delta\tau = 0{\cdot}12$ after the impact is given in the center-plot, where it is also sketched the direction of the incoming water. The right plot gives the maximum tension and compression bending stresses. Compression stresses reach larger values than tension ones. This is because the cross-sectional neutral axis is closer to the wetted side. We note that magnitude of hydroelastic results oscillates around a mean value close and above the quasi-steady analysis. This documents the unimportance of hydroelasticity in this case.

This research activity has taken place at the Strong Point Centre on Hydroelasticity in Trondheim, supported by NTNU and MARINTEK. The research has also been supported by the Italian *Ministero dei Trasporti e della Navigazione* through INSEAN Research Program 2000-02. The mobility of M.L. is partly supported by ONR through University of Hiroshima.

REFERENCES

Cozijn, J. L., " Development of a calculation tool for green water simulation", MARIN Wageningen / Delft Univ. of Technology, the Netherlands, 1995.

Ersdal, G. & Kvitrud, A., "Green water on Norwegian production ships", Proc. 10^{th} Int. Conf. Offshore and Polar Engg, ISOPE'2000, Seattle, 2000.

Faltinsen, O.M., "Hydroelastic slamming", J. Marine Science and Technology, Vol. 5, No. 2, 2001.

Greco, M., Faltinsen, O.M. & Landrini, M., "Basic Studies of Water on Deck", Proc. 23^{rd} Symp. on Naval Hydrod., Val de Reuil, National Academy Press, Washington D.C., 2000.

Tanizawa, K., "A Numerical Simulation Method of Hydroelastic Water Surface Impact Based on Acceleration Potential", Proc. FEDSM99, 3^{rd} ASME/JSME Joint Fluids Eng. Conf., San Francisco, 1999.

Zhao, R. & Faltinsen, O.M., "Water Entry of arbitrary Axisymmetric Bodies With and Without Flow Separation", Proc. 22^{nd} Symp. on Naval Hydrod., National Academy Press, Washington D.C., 1998.